Motion of Nanodroplets near Edges and Wedges

A. Moosavi, M. Rauscher,* and S. Dietrich

Max-Planck-Institut für Metallforschung, Heisenbergstrasse 3, D-70569 Stuttgart, Germany

Institut für Theoretische und Angewandte Physik, Universität Stuttgart, Pfaffenwaldring 57, D-70569 Stuttgart, Germany

(Received 14 September 2006; published 6 December 2006)

Nanodroplets residing near wedges or edges of solid substrates exhibit a disjoining pressure induced dynamics. Our nanoscale hydrodynamic calculations reveal that nonvolatile droplets are attracted or repelled from edges or wedges depending on details of the corresponding laterally varying disjoining pressure generated, e.g., by a possible surface coating.

DOI: 10.1103/PhysRevLett.97.236101 PACS numbers: 68.08.Bc, 68.15.+e, 68.35.Ct

Wetting phenomena [1,2] and thin film dynamics [3] on rough [4] or topographically structured [5,6] substrates have been studied in detail both experimentally [5–8] and theoretically [4,9,10]. To a large extent these investigations are motivated by the fact that generically substrates are rough, in particular, those playing an important role in technological processes such as oil recovery, coating, lubrication, and paper processing. A second driving force for the progressive application of these micro and nanofluidic processes stems from the lab-on-a-chip concept which integrates pipes, pumps, reactors, and analyzers into a single device allowing for a cost efficient handling of minute amounts of liquid containing, e.g., DNA or proteins [11].

Most theoretical investigations of wetting of structured substrates have been concerned with thermal equilibrium. Only recently efforts have been made towards understanding the corresponding dynamics. Using various numerical techniques, time-dependent free surface flow over topographic features has been investigated [12–15]. However, the applicability of these results to the nanoscale is impeded because the effect of intermolecular interactions, relevant at the nanoscale, either has not been considered [12,13] or only in a rather crude way [14,15].

In contrast, here we study nanoscale fluid dynamics on topographical surface structures by properly taking into account the spatial variation of the long-ranged intermolecular interactions. We focus on edges and wedges as two paradigmatic geometric structures and provide a detailed dynamical study of their effects on nanodroplets positioned in their vicinity. We consider a partially wetting, nonvolatile, and incompressible liquid film composed of a nanodroplet on top of a precursor wetting layer on a possibly coated solid substrate [16]. Our analysis shows that the dynamics of droplets on such structures depends on subtle details of the substrate properties.

For given intermolecular interactions, based on density functional theory the free energy of a prescribed liquid film configuration in contact with, e.g., a wedgelike substrate is a functional of the liquid-vapor interface shape [17] which can be expressed in terms of the so-called effective interface potential ω [17,18]. For a flat substrate and film thickness h one has $\omega(h) = -\int_h^\infty \Pi(y)dy$, where Π is the disjoining pressure (DJP). Since the equation of motion can be expressed in terms of Π, we determine Π directly following Ref. [16]. Assuming Lennard-Jones type pair potentials $V_{\alpha\beta}(r) = M_{\alpha\beta}/r^{12} - N_{\alpha\beta}/r^6$, where $M_{\alpha\beta}$ and $N_{\alpha\beta}$ are material parameters, and α and β relate to liquid (l), substrate (s), or coating (c) particles, the DJP corresponding to chemically homogeneous substrate is given by [19]

$$\Pi(\mathbf{r}) = \int_{\Omega_s} [\rho_l^2 V_{ll}(\mathbf{r} - \mathbf{r}') - \rho_l \rho_s V_{sl}(\mathbf{r} - \mathbf{r}')] d^3 r' \quad (1)$$

with $\mathbf{r} = (x, y, z) \in \mathbb{R}^3$, and ρ_l and ρ_s are the number densities of the liquid and the substrate, respectively. Ω_s is the substrate volume. Equation (1) assumes that the vapor density is so low that its contribution to Π can be neglected. For a noncoated edge $\Omega_s = \{\mathbf{r} \in \mathbb{R}^3 \mid x, y \leq 0, z \in \mathbb{R}\}$ (see Fig. 1) this yields

$$\Pi_e(x, y) = \int_{\Omega_s} \frac{\Delta M}{|\mathbf{r} - \mathbf{r}'|^{12}} d^3 r' - \int_{\Omega_s} \frac{\Delta N}{|\mathbf{r} - \mathbf{r}'|^6} d^3 r', \quad (2)$$

where $\Delta M = \rho_l^2 M_{ll} - \rho_l \rho_s M_{sl}$ and $\Delta N = \rho_l^2 N_{ll} - \rho_l \rho_s N_{sl}$. The first (second) term dominates near (far from) the substrate. On a flat and homogeneous substrate the equilibrium thickness of the wetting layer is given by the zero of Π which corresponds to the minimum of ω. For the interactions considered here, $\Delta M \geq 0$ is a necessary condition for the occurrence of an equilibrium wetting layer of nonzero thickness. Both integrals in Eq. (2) can be calculated analytically and one obtains the DJP as the corresponding difference of two contributions $\Pi_e = \Pi_e^{12} - \Pi_e^6$.

In order to enrich the model we consider in addition the case that the substrate is covered by a thin coating layer of thickness d. Actual coating layers have a more complicated structure, in particular, around edges or wedges, which depends on the specific combination of coating and substrate material as well as how the coating is deposited. Such details do influence the motion of droplets very close to the edge but corresponding calculations carried out by us indicate that a simple model with rather small d captures correctly the dynamics at lateral distances from the edge larger than d. The contribution of a thin coating layer to the

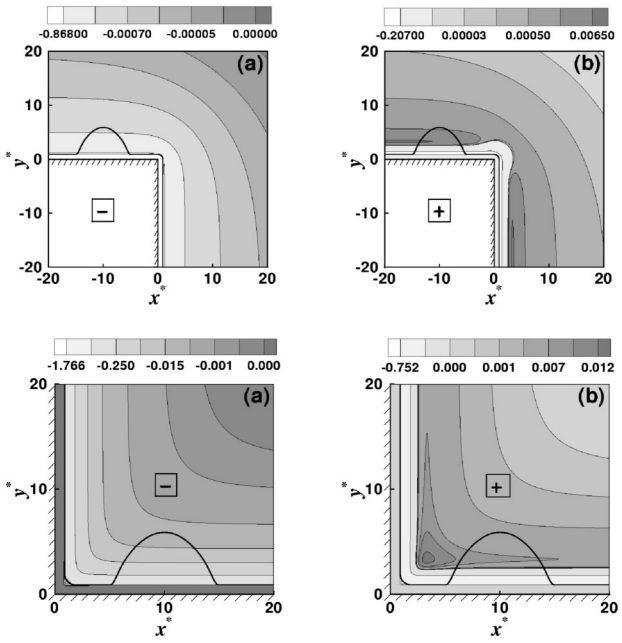

FIG. 1. Edge (top) and wedge (bottom) configurations. A nanodroplet (full line) is placed near these geometrical structures and thus it is exposed to the action of the laterally varying DJP. Contour plots of the corresponding dimensionless DJP for the minus [(a) $B = -1$, $C = 1$)] and plus [(b) $B = -2.5$, $C = 1$)] case are shown [see Eq. (3)].

DJP can be determined as above, assuming a van der Waals type interaction between the coating and the liquid particles. We do not consider an additional repulsive part of the liquid-coating interaction as this is shorter ranged ($\sim y^{-10}$) than the corresponding part $\Pi_e^{12} \sim y^{-9}$ [16,18]. The contribution $\Pi_c^u(x, y)$ of the coating layer on the horizontal *u*pper part of the edge $\{(x, y, z)|x < 0, y = 0\}$ to the DJP can also be calculated analytically. By symmetry, the contribution of the vertical coating layer is $\Pi_c^u(y, x)$. Thus the DJP with the coating is $\Pi_{ce}(x, y) = \Pi_e(x, y) + \Pi_c^u(x, y) + \Pi_c^u(y, x)$.

Far from the edge, i.e., for $x \to -\infty$, the DJP reduces to that of a coated *f*lat substrate: $\Pi_{cf}(y) = \pi\Delta M/(45y^9) - \pi\Delta N/(6y^3) + \pi\Delta N' d/2y^4$, with $\Delta N' = \rho_l^2 N_{ll} - \rho_l\rho_c N_{cl}$ measuring the interaction strength of the coating layer. We introduce dimensionless quantities (marked by $*$) such that lengths are measured in units of $b = [2\Delta M/(15|\Delta N|)]^{1/6}$ which for $\Delta N > 0$ is the equilibrium wetting film thickness on the uncoated flat substrate. For the relation between b and the equilibrium wetting film thickness on the coated substrate, see the insets in Fig. 2. The DJP is measured in units of the ratio σ/b where σ is liquid-vapor surface tension. Thus the dimensionless DJP $\Pi_{cf}^* = \Pi_{cf} b/\sigma$ far from the edge has the form

$$\Pi_{cf}^*(y^*) = C\left(\frac{1}{y^{*9}} \pm \frac{1}{y^{*3}} + \frac{B}{y^{*4}}\right). \tag{3}$$

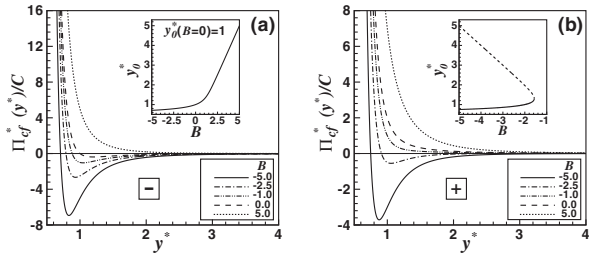

FIG. 2. Rescaled DJP far from the edge in the plus (a) and the minus (b) case for different B [see Eq. (3)]. The insets show the positions of the zeros of Π_{cf}^* as a function of B. In the plus case Π_{cf}^* has zeros only for $B < -1.57$. The full curves in the insets correspond to the equilibrium wetting layer thickness.

The dimensionless amplitude $C = Ab/\sigma$, where $A = \pi(\Delta M/45)^{-1/2}(|\Delta N|/6)^{3/2}$, compares the strengths of the effective intermolecular forces in the uncoated case and of the surface tension forces. The amplitude $B = \pi\Delta N' d/(2Ab^4)$, which can be positive or negative, measures the strength of the coating layer. Note that an analysis of the DJP, which is more refined than Eq. (1), yields $B \neq 0$ even in the absence of a coating layer [2,18]; therefore, in the following we consider B as an independent parameter. In the second term on the right-hand side of Eq. (3) the upper (lower) sign corresponds to $\Delta N < 0$ ($\Delta N > 0$). In the following we shall refer to these cases as the plus and the minus case (see Fig. 2). In the minus case, the DJP has a single zero for all B, while in the plus case there is no zero for $B > -1.57$ and two zeros for $B < -1.57$. The dimensionless form of the DJP for a coated edge is given by

$$\Pi_{ce}^*(x^*, y^*) = C\left\{\frac{45\Pi_e^{12}(x^*, y^*)}{\pi\Delta M} \pm \frac{6\Pi_e^6(x^*, y^*)}{\pi|\Delta N|} + \frac{2B[\Pi_c^u(x^*, y^*) + \Pi_c^u(y^*, x^*)]}{\pi|\Delta N'|}\right\}. \tag{4}$$

The physically possible ranges of C and B in these cases can be inferred from considering the macroscopic equilibrium contact angle $\theta_{\rm eq}$ given by $\cos\theta_{\rm eq} = 1 + \omega_{cf}^*(y_0^*)$ with y_0^* being the minimum of the corresponding effective interface potential $\omega_{cf}^*(y^*) = \int_{y^*}^{\infty} \Pi_{cf}^*(y')dy'$ [2]. $|\cos\theta_{\rm eq}| \leq 1$ implies $B < -1.87$ for the plus case so that the disjoining pressure has two zeros. In the minus case there is no limitation for B.

Figure 1 shows a typical example of the DJP at an edge for both the minus and the plus case, respectively. If a droplet is placed near the edge, it is exposed to the lateral gradient of the disjoining pressure resulting in a lateral force on the droplet. In the following we restrict our analysis to ridges translationally invariant along z, expecting that our arguments and conclusions carry over qualitatively to actual three-dimensional droplets. For a ridge, the lateral force density on the droplet is $f^* = \frac{1}{\Omega_d^*} \times \int_{\partial\Omega_d^*} \Pi_{ce}^*(x^*, y^*) n_{x^*} dS^*$. $\partial\Omega_d^*$ and Ω_d^* are the dimension-

less droplet surface and volume, respectively, and n_{x^*} is the x^* component of the unit surface normal vector pointing outward. In Fig. 3 this force density, estimated by the force density on a parabolic droplet crossing over smoothly to a wetting layer of thickness y_0^* (discussed as initial configuration for the Stokes dynamics below, see also Fig. 1), is plotted as a function of the distance w^* (see Fig. 4) between the three-phase contact line and the edge for different values of B. For the minus case there is a critical value $B_c \approx -10$ which depends weakly on the drop size. For $B > B_c$ the force is always positive and increases towards the edge. Thus one expects the droplet to move towards the edge. However, for $B < B_c$ the force changes sign from plus to minus upon approaching the edge and the droplet will stop at a certain distance from the edge which increases with decreasing B. In the plus case the force is always pointing away from the edge, and becomes stronger upon approaching the edge. Therefore, in this case one expects a droplet to move away from the edge.

We analyze the liquid flow of this motion in terms of a two-dimensional Stokes equation. In dimensionless form the continuity and Stokes equation read $\nabla \cdot \mathbf{u}^* = 0$ and $C\nabla^2 \mathbf{u}^* = \nabla(p^* + \Pi^*)$, where $\mathbf{u}^* = (u_{x^*}^*, u_{y^*}^*)$ is the velocity vector and p^* is the hydrostatic pressure. The velocity and time scales are Ab/μ and μ/A, respectively, with the viscosity μ. Lengths and pressure have been scaled with b and σ/b, respectively. At the liquid-solid interface a no-slip condition is applied and there is no flux into the impermeable substrate. Along the liquid-vapor interface the tangential stresses are zero (neglecting the viscosity of the vapor phase) and normal stresses are balanced by the pressure, the DJP, and the surface tension [13,20]. There is no flux through the boundaries of the box used for the numerical calculations, guaranteeing mass conservation. We solve these equations numerically with a standard biharmonic boundary integral method [13,20] for initial droplet shapes of the form $y^*(x^*; t = 0) = y_0^* + a^*\{1 - [(|x^*| - g^*)/a^*]^2]\}^{||x^*|-g^*|^m+1}$. a^* is the droplet height in the center and half the basewidth, and g^* is the distance of the droplet center from the edge. In this study m was chosen to be 10. At $t = 0$ the droplet is positioned with its three-phase contact line $[x^* = -(g^* - a^*), y^* = y_0^*, z^*]$ at a distance $w^* = g^* - a^*$ away from the edge (see Fig. 4).

Figure 4 illustrates the difference of the motion of the droplets in the minus and the plus case for values of B and C chosen such that in both cases $\theta_{eq} = 90°$. (Thus the present dynamics is complementary to the motion of droplets caused by chemically generated contact angle gradients [21].) The droplet moves towards the edge in the minus case and away from the edge in the plus case. The motion towards the edge in the minus case accelerates but comes to a stop when the right three-phase contact line of the drop reaches the edge. In the plus case, the drop motion decelerates but does not stop.

As a second system we consider a wedgelike substrate. A wedge can be viewed as being composed of a flat vertical substrate and an edge. Thus, combining their contributions yields $\Pi_{cw}^*(x^*, y^*) = \Pi_{cf}^*(x^*) - \Pi_c^{u*}(y^*, x^*) + \Pi_e^*(-x^*, y^*) + \Pi_c^{u*}(-x^*, y^*)$. For a noncoated wedge, within our model this is in accordance with Ref. [17]. Typical examples of the DJP in the wedge for the minus and the plus cases are depicted in Fig. 1. For different values of B the DJP induced lateral force on a parabolic ridge is shown in Fig. 3 for the minus and the plus case, respectively. The force is always positive, i.e., pointing away from the wedge for the minus case with its strength decreasing with distance. Thus, one expects a droplet to move away from the wedge. For the plus case the force changes sign from

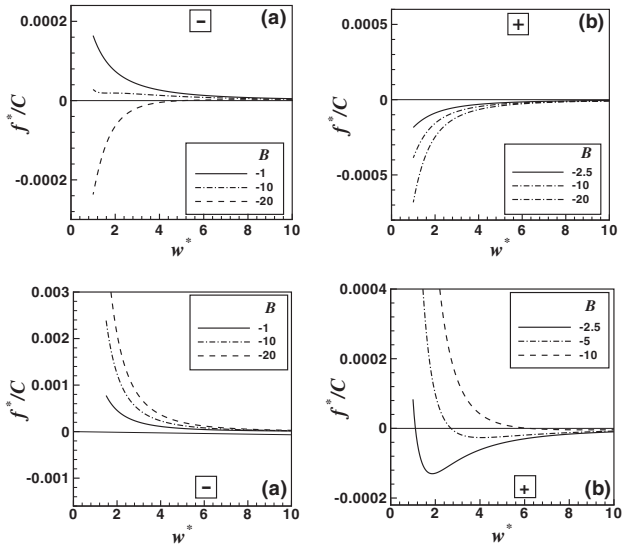

FIG. 3. Normalized DJP induced lateral force densities f^* acting on an initial droplet configuration (see Fig. 1) of height $a^* = 15$ and at distance w^* (see Fig. 4) from an edge (top) and a wedge (bottom) for the minus (a) and the plus (b) case.

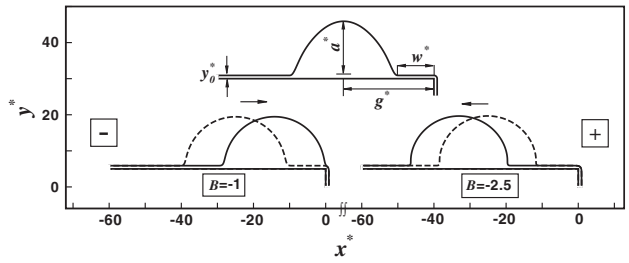

FIG. 4. Motion of a droplet ($a^* = 15$, $w^* = 10$) near an edge for the minus (lower left, $B = -1$, $C = 1.27$) and the plus (lower right, $B = -2.5$, $C = 4.23$) case. For y_0^* see the insets in Fig. 2. The upper figure shows the initial droplet shape. Shown are interface profiles at $t^* = 339$ (dashed line) and $t^* = 20\,893$ (solid line) for the minus case and at $t^* = 210$ (dashed line) and $t^* = 93\,699$ (solid line) for the plus case. The chosen values of B and C provide $\theta_{eq} = 90°$.

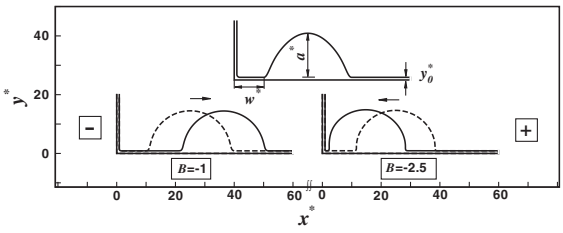

FIG. 5. Motion of a droplet ($a^* = 15$, $w^* = 10$) near a wedge for the minus (lower left, $B = -1$, $C = 1.27$) and the plus (lower right, $B = -2.5$, $C = 4.23$) case. For y_0^* see the insets in Fig. 2. The upper graph shows the initial droplet shape. Shown are interface profiles at $t^* = 450$ (dashed line) and $t^* = 99\,750$ (solid line) for the minus and $t^* = 160$ (dashed line) and $t^* = 14\,683$ (solid line) for the plus case. The chosen values of B and C provide $\theta_{eq} = 90°$.

negative to positive near the wedge at a distance which increases with decreasing B. Thus one expects the droplet to move towards the wedge and then to stop before reaching the wedge. This is indeed what is observed in the numerical calculations of a liquid ridge as shown in Fig. 5. The droplet moves away from the wedge with decreasing speed in the minus case and towards the wedge with increasing speed in the plus case. However, in the plus case the droplet stops before it reaches the wedge. Only if the droplet is driven into the wedge (e.g., by external forces) or if it touches the wedge during the initial relaxation process, the droplet gets trapped in the wedge and forms a configuration symmetric with respect to the bisector of the wedge.

In summary, we have shown how topographic substrate features generate motion of nonvolatile nanodroplets residing in their vicinity. This motion depends on the details of the interplay between the liquid-liquid and the liquid-substrate interactions. This resembles similar phenomena occurring near chemical heterogenities [22]. Taking 1 nm and 0.02 N/m as typical values of b and σ, respectively, and for the values of C and B chosen in Figs. 4 and 5, our model calculations predict that near an edge the DJP induced lateral force on a liquid ridge 30 nm long, 15 nm high, and 1 nm thick is of the order of 10^{-13} N. For this droplet size the gravitational body force is about 8 orders of magnitude smaller. Only for micron-sized drops the gravitational force becomes competitive. The time scale μ/A for the motion is roughly $[10^{-8}\mu/(\mathrm{Pa\,s})]$ s so that the average velocities for the cases studied are ca. $\{10^{-5}/[\mu/(\mathrm{Pa\,s})]\}$m/s. Taking μ between 0.1 Pa s and 100 Pa s (different polydimethylsiloxanes at ambient temperature) the velocity ranges from 0.1 mm/s to 0.1 μm/s, which is comparable with the velocities of droplets of the same kind of liquid but exposed to and driven by a chemical step generated by a contact angle contrast of a few degrees [21]. Our calculations indicate that relaxation of the droplet radius is faster than the motion of the droplet as a whole which leads to the expectation that the velocity of precursor spreading is larger than the droplet motion [23].

Our findings have a bearing on the distribution of droplets after condensating liquid onto nanosculptured substrates and on breath figures, in addition to possible implications for the design of open nanofluidic systems in which the activating force, partially or totally, is provided by the system itself.

M. R. acknowledges DFG support under Grant No. RA 1061/2-1 (SPP 1164).

*Electronic address: rauscher@mf.mpg.de

[1] P. G. de Gennes, Rev. Mod. Phys. **57**, 827 (1985).
[2] S. Dietrich, in *Phase Transitions and Critical Phenomena*, edited by C. Domb and J. L. Lebowitz (Academic, New York, 1988).
[3] A. Oron, S. H. Davis, and D. G. Bankoff, Rev. Mod. Phys. **69**, 931 (1997).
[4] R. R. Netz and D. Andelman, Phys. Rev. E **55**, 687 (1997).
[5] L. Bruschi, A. Carlin, and G. Mistura, Phys. Rev. Lett. **89**, 166101 (2002).
[6] O. Gang, K. J. Alvine, M. Fukuto, P. S. Pershan, C. T. Black, and B. M. Ocko, Phys. Rev. Lett. **95**, 217801 (2005).
[7] J. Klier, P. Leiderer, D. Reinelt, and A. F. G. Wyatt, Phys. Rev. B **72**, 245410 (2005).
[8] T. Ondarçuhu and A. Piednoir, Nano Lett. **5**, 1744 (2005).
[9] K. Rejmer, S. Dietrich, and M. Napiórkowski, Phys. Rev. E **60**, 4027 (1999).
[10] C. Rascón and A. O. Parry, Nature (London) **407**, 986 (2000).
[11] G. Karniadakis, A. Beskok, and N. Aluru, *Microflows and Nanoflows: Fundamentals and Simulation* (Springer, New York, 2005), 2nd ed.
[12] P. H. Gaskell, P. K. Jimack, M. Sellier, and H. M. Thompson, Phys. Fluids **18**, 013601 (2006).
[13] C. M. Gramlich, A. Mazouchi, and G. Homsy, Phys. Fluids **16**, 1660 (2004).
[14] P. H. Gaskell, P. K. Jimack, M. Sellier, and H. M. Thompson, Int. J. Numer. Meth. Fluids **45**, 1161 (2004).
[15] C. Bielarz and S. Kalliadasis, Phys. Fluids **15**, 2512 (2003).
[16] C. Bauer and S. Dietrich, Phys. Rev. E **60**, 6919 (1999).
[17] M. Napiórkowski, W. Koch, and S. Dietrich, Phys. Rev. A **45**, 5760 (1992).
[18] S. Dietrich and M. Napiórkowski, Phys. Rev. A **43**, 1861 (1991).
[19] M. O. Robbins, D. Andelman, and J. F. Joanny, Phys. Rev. A **43**, 4344 (1991).
[20] M. A. Kelmanson, J. Eng. Math. **17**, 329 (1983).
[21] E. Raphaël, C. R. Acad. Sci. Paris Ser. II **306**, 751 (1988).
[22] M. K. Chaudhury and G. M. Whitesides, Science **256**, 1539 (1992).
[23] D. R. Heine, G. S. Grest, and E. B. Webb III, Phys. Rev. Lett. **95**, 107801 (2005), and references therein.